Silicon (2022) 14:4391–4400
https://doi.org/10.1007/s12633-021-01229-7

ORIGINAL PAPER

Dosimetric impact of some gamma radiation-induced polymeric materials incorporated silicate using thermoluminescence and ultrasonic techniques

M. Afifi[1] · M. R. Abass[2] · H. M. Diab[3] · M. M. Abou-Mesalam[2] · M. S. Gaafar[1]

Received: 11 March 2021 / Accepted: 22 June 2021 / Published online: 2 July 2021
© Springer Nature B.V. 2021

Abstract
Polyacrylamide acrylonitrile magnesium silicate {P(Am-AN)-MgSi} & polyacrylamide acrylic acid magnesium silicate {P(Am-AA)-MgSi} hybrid composites were fabricated utilizing gamma-radiation polymerization initiated about 30 kGy. Different types of dosimetric radiation-induced polymeric composites were irradiated by cesium-137 gamma-ray dose to show its possibility for use as a thermoluminescence dosimeter. The prepared polymeric composites showed useful properties such as good dosimetric and thermal stability behaviors. The mechanical behavior of the samples was measured non-destructively by the ultrasonic pulse-echo technique. It was found that the addition of P(Am-AA) with higher elastic moduli to MgSi with lower ones are produced in the {P(Am-AA)-MgSi} composite sample with a midway value for Young's modulus of 7.13 GPa and shear modulus of 2.71 GPa. Dissimilar in the {P(Am-AN)-MgSi} composite sample, it shows a significantly improved behavior as Young's modulus recorded 9.32 GPa and shear modulus 3.61 GPa. Similarly, the microhardness recorded 0.328 GPa and 0.518 GPa a the composites {P(Am-AN)-MgSi} & {P(Am-AA)-MgSi}. As a thermoluminescence dosimeter, various characteristics were studied for these types of polymers. Specific ultrasonic properties were also tested for TL dosimetric properties in different polymers. An insertion of MgSi into P(Am-AN) & P(Am-AA) has indeed been found to increase TL response and lead to good properties being acquired.

Keywords Magnesium Silicate · Gamma-Radiation · Thermoluminescence · Young's modulus · Ultrasonic mechanical behavior

1 Introduction

Thermoluminescence (TL) is the instinctive emission of light by a material when it is heated. This material was previously exposed by ionizing radiation such as γ-rays, X-rays, etc., where the ionizing radiation established traps and voids to the material and filled them energy presented as electrons and holes. When applying heat to this material, the electrons and holes migrate freely in the material lattice till they recombine or fill other traps and resulting photon emission. The materials can present a peak of the emitted light intensity (I_{TL}) by changing the material's temperature together with a linear increase of the maximum peak height with increasing the irradiation dose could be used as a dosimeter. Therefore, to measure the absorbed dose by a dosimeter, a calibration curve between I_{TL} and the absorbed dose is required.

M. Mirzayev et al. [1] investigated the effect of gamma irradiation on the surface morphology and crystalline structure of boron carbide (B_4C). The results indicate the amorphous phase in B4C structure has increased with gamma irradiation, which is due to the weakening of the C–C bonds with respect to the B–C bonds. M. Mirzayev [2] studied the effect of Co^{60} gamma irradiation on the oxidation kinetics of the ultra-pure boron carbide ceramic. He found a rise in the activation energy from 99.6 J.mol^{-1} to 102.9 J.mol^{-1} with an increase in the irradiation dose from $5{\cdot}10^6$ to $2{\cdot}10^7$ Mrad. In the same manner, the silicide hexaboride [3] has shown a good thermoluminescence response as the activation energy is inversely proportional with the γ-ray irradiation dose, which also affects the lattice volume.

✉ M. Afifi
Mahmoud@daad-alumni.de; phafifi@gmail.com

[1] Ultrasonic Laboratory, National Institute of Standards, Giza, Egypt

[2] Egyptian Atomic Energy Authority, Hot Laboratories Centre, 13759 Cairo, Egypt

[3] Ionizing Radiation Metrology Laboratory, National Institute of Standards, Giza, Egypt

Nowadays, many types of research showing the dosimetric effect of low absorbed doses in different materials as utilization for the new materials [4, 5]. The thermoluminescent (TL) properties of polymers have been widely studied [6, 7]. The grafted polymer is commonly employed as radiation dosimetry measurement material because of its higher sensitivity, resistivity to radiation damage [8]. Moreover, it can be used to reflect a high spatial resolution in very small sizes. It has been reported for dosimetric characteristics of different diamond samples as well [8]. Grafted polymers, after exposure to a cesium-137 gamma irradiation beam, revealed an excellent TL sensitivity. The dose-response is linear until 3 Gy. Due to high thermal fading, which is caused by the presence of lower-temperature peaks in glow curves, the need has arisen to seek new materials with different defect types. A group of radiation-induced polymer samples was studied to detect the TL response with better accuracy. The dosimetric characterization of suggested polymers contains the TL response as dose-dependence integral values and peak heights, the radiation energy dependent on the TL response, and the thermal fading process [9].

The particular control of electrons and photons from outer sources is accomplished by [6, 7], and it is regarded as one of the uses of thermoluminescence for dosimetry. One can conclude many error sources that can judge the accuracy and precision in calculating the dose under a definite geometrical state [10]. Uses of irradiated ^{60}Co gamma-ray dose solar cells were achieved and revolved that the monocrystalline silicon solar cell system is considered to be a substantial material for the determination of gamma dosimetry due to the improvement in the TL response [10]. Also, the different uncertainty sources in radiation dosimetry were analyzed, which concluded that: expanded uncertainty value at a 95 % confidence level has to gather with the TL response measurement values to obtain correct doses [10, 11].

The material's mechanical properties are often fundamental in research to determine the material's best use in applications. The traditional way to determine such properties needs a sample with unique dimensions and causes material changes as it is destructive testing such as flexural and tensile testing. Moreover, many materials are inline in a production process like polymers. Most polymers are characterized by time-dependent mechanical properties and need to be determined non-destructively [12]. However, ultrasonic techniques are widely used to investigate the material's mechanical properties based on the wave's speed propagate inside it [13]. The ultrasonic technique's advantages can be concluded as inline operation, low cost, and flexibility with test sample geometry.

Moreover, the experiment results showed that thermoluminescence tellurite examination demonstrated that a tellurite's potential can be used as a material for gamma-ray thermoluminescence [14] and is beneficial at radiation doses used for therapeutic purposes [15]. This study target is to better understand the response of polymer composites prepared by gamma radiation at 30 kGy with and without added MgSi to gamma radiation dose measurements to check the possibility of using these mentioned polymers as a gamma radiation dosimeter. The materials used in this paper were used previously for various uses, such as toxic metal ions removal from industrial & radioactive waste [16] and optical bandgap enhancement [17].

2 Experimental

2.1 Materials

$MgCl_2.6H_2O$; 99 %, Na_2SiO_3, 99 %, and acrylamide solution; 40 % (Am: C_3H_5NO), (Alpha Chemika, India), acrylonitrile solution; 0.5 mg/mL in methanol (AN: C_3H_3N), and acrylic acid; 99 % (AA: $C_3H_4O_2$), (Merck, Germany) and acetone; 99.5 % (Aldrich, Germany). All chemicals were analytical grade and used without further purification with a micro-scale in size. Distilled water was utilized for preparing composites and solutions used.

2.2 Gamma Cell

A radiation source Co^{60} gamma cell (Category MC-20, Russia), located at Cyclotron Project, Inshas, Egypt, was used for polymerization. At 25 ± 1 °C, a sample was irradiated. A source of irradiation has a dosage rate of 460.7 Gy/h.

2.3 Methods

Magnesium silicate was provided by an additional drop of 0.1 M Na_2SiO_3 solution to 0.1 M $MgCl_2.6H_2O$ in this sample, which has a volumetric ratio of Mg/Si = 1.5 at constant agitation at 25 ± 1 °C. A precipitate was washed away with diluted HNO_3 to remove Cl^- and impurities. A precipitate was then re-washed with deionized water to extract NO_3^-. It was filtered, then washed in deionized water several times. A precipitate was dehydrated overnight at about 50–60 °C and sewn to achieve a uniform particle size [17].

By dropwise addition with volumetric ratio equal unity to acquire (Am + AN) & (Am + AA) co-monomers, a solution of Am monomer was combined with a solution of AN and AA. (Am + AN) and (Am + AA) co-monomers were then combined dropwise with solutions of 0.1 M Na_2SiO_3 and 0.1 M $MgCl_2.6H_2O$. A volumetric ratio was adjusted to 1:1:1.5:1 for (Am-AN-Mg-Si) & (Am-AA-Mg-Si). A mixture was produced by agitating for 3 h at 30 °C. To obtain the P(Am-AN), P(Am-AA), {P(Am-AN)-MgSi} and {P(Am-AA)-MgSi} composites, these co-monomers were subjected to gamma irradiation at 30 kGy over a time of about 65 h and normal temperature. After irradiation, a resultant hydrogel

was crushed into small fragments followed by agitation with acetone to eliminate unreacted compounds and dried at 60 °C.

2.4 Characterization

On a spectrometer model 2000 FTIR, Perkin Elmer Corporation, USA, IR spectra were analyzed at 400–4000 cm^{-1}. The sample micrographs were investigated via field emission SEM (model JSM-5400, JEOL Instrument, Japan). The FESEM was operated under an accelerating voltage of 10 kV. Each sample's powder has been mixed using agate mortar for 30 min to ensure homogeneous distribution of the initial compounds. For the mechanical and compactness investigations, the mixed powders were pressed using a uniaxial press at 15 tons for 2 min each. The compressed disks were exposed to high-power ultrasonic waves using (Branson 450 digital signifier) in silicon oil for 20 min at 40 W. The mechanical properties were studied non-destructively before and after the exposer to investigate the effect of beating high-power sound waves and cavitation on the prepared samples. The mechanical performance of prepared samples was measured using the ultrasonic pulse-echo technique (UT) using (USN60 flaw detector) based on the determination of both longitudinal (L) and shear (v_S) wave velocities inside the samples. The flaw detector, with a transducer connected to it, can measure the ultrasonic waves traveling time (Δt); 4 MHz transducer (Karl Deutsch S12-HB4) for longitudinal waves and 2 MHz (KrautKramer K2KY) for shear waves. Using the sample thickness (h), the velocity can be calculated using v = 2 h/Δt. The longitudinal modulus (L), shear modulus (G), Young's modulus (E), bulk modulus (K), microhardness (H), and Poisson's ratio (ν) can be calculated using the following equations [18, 19]

$$L = \rho v_L^2, \tag{1}$$

$$G = \rho v_S^2, \tag{2}$$

$$K = L - \frac{4G}{3}, \tag{3}$$

$$E = (1+\nu)2G, \tag{4}$$

$$H = \frac{(1-2\nu)E}{6(1+\nu)} \text{ and} \tag{5}$$

$$\nu = \frac{L-2G}{2(L-G)} \tag{6}$$

where ρ is the density of samples.

The planchet heating Harshaw 4500 Reader method is used for measuring The TL response. A stainless steel crucible that is in contact with the sample is used to heat the samples; the monitoring of the temperature was done by placing the thermocouple in close interaction with the sample holder. Samples are heated with a heating rate of 2 °C/s inside a temperature range from 50 °C up to 400 °C after irradiation. The used technique to verify the complete formation of the sample with no extra heat treatment is required [8]. The dosimetric properties were achieved with (cesium 137) photons source at the National Institute of standards, Egypt. The IAEA code of practice is used for dose determination [20, 21], with an expanded uncertainty of about 2 %.

3 Results and Discussion

3.1 FTIR

Figure 1. shows the IR spectra of MgSi, P(Am-AN), P(Am-AA), {P(Am-AN)-MgSi} & {P(Am-AA)-MgSi} composites. Six characteristic bands, were noted for MgSi. ~ 3150–3670, and ~ 1652 for stretching & bending vibration of water & OH absorbed on MgSi [16, 22]. ~ 1000–1100, for (Mg-O) [23, 24]. ~ 903, for Mg-OH deformation vibration [25]. ~ 640 & 470 cm^{-1} are agreed to Si-O-Mg & Si-O-Si bending vibrations, respectively [26] as in Table 1.

IR spectra for P(Am-AN) & {P(Am-AN)-MgSi} composites fabricated at 30 kGy show that two bands appeared at 3340–3450 & 3195 cm^{-1} for a stretching vibration for N-H of acrylamide & H-O-H, respectively [27, 28]. (2935 & 2875 cm^{-1}) and (1450 & 1409 cm^{-1}) to stretching & bending vibrations for asymmetric & symmetric CH_2 of acrylamide & acrylonitrile, respectively [28–31]. 2244 cm^{-1} for C ≡ N of acrylonitrile [29, 30]. 1665 cm^{-1} for C = O of amide I [32]. 1605 cm^{-1} for the C-N-H bond of acrylamide bending [32]. 1182 & 1120 cm^{-1} to asymmetric and symmetric C-N the bending vibration [28, 29]. 1040, 905, 636 & 460 cm^{-1} for

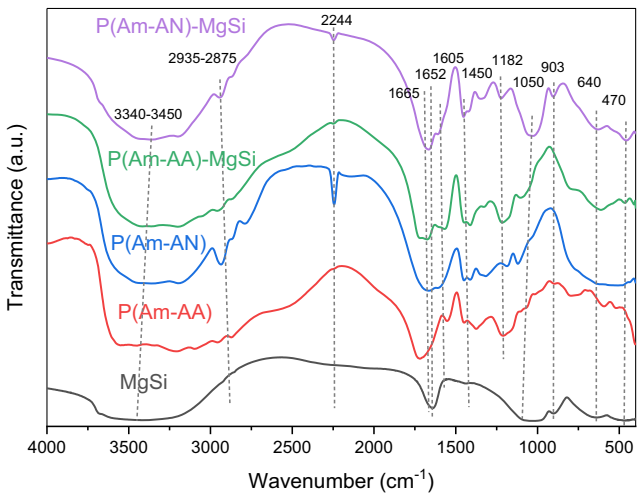

Fig. 1 IR spectra of (**A**) MgSi, P(Am-AN), and {P(Am-AN)-MgSi} composites and (**B**) MgSi, P(Am-AA), and {P(Am-AA)-MgSi} composites

Table 1 Assignments of IR bands (cm^{-1}) of MgSi, P(Am-AN), P(Am-AA), {P(Am-AN)-MgSi} & {P(Am-AA)-MgSi} composites

Wavenumber (cm^{-1})	Assignments	References
3340–3450	γ N-H	[27, 28]
3150–3670	γ OH and γ. H_2O	[27, 28]
2935,2875	γ CH_2 (asymmetric and symmetric)	[28–31]
2244	γ C≡N	[29, 30]
1665	C=O in the amide I	[32]
1652	δ. H_2O	[16, 22]
1605	δ. C-N-H	[32]
1605,1571	δ. C-N-H (asymmetric and symmetric)	[32]
1450,1409	δ. Of C-H in CH_2 (asymmetric and symmetric)	[28–31]
1182,1120	δ. C-N (asymmetric and symmetric)	[28, 29]
1000–1100	δ. (Si-O) or Si-O-Si	[33–35]
903	δ. Si-OH or Si-CH_2	[16, 26, 35]
640	δ. Si–O–Mg	[16, 26]
470	δ. Si-H	[35]

{P(Am-AN)-MgSi} to Si-O [33, 34] or Si-O-Si [35], Si-OH deformation vibration [16, 26] or Si-CH_2, Si-O-Mg [16, 26] and Si-H [35], respectively. A fourth later absorption bands confirmed that impregnation of Mg & Si in a structure of polymeric resin.

Figure 1 show IR spectra for P(Am-AA) & {P(Am-AA)-MgSi} composites produced at 30 kGy. Bands appeared at 3450 & 3354 cm^{-1} to N-H & O-H stretching vibration [36, 37]. (2950 & 2870 cm^{-1}) and (1450 & 1370 cm^{-1}) to stretching & bending vibrations of asymmetric & symmetric CH_2 of acrylamide & acrylic acid [38]. 1720 cm^{-1} to amide I [39]. 1550 cm^{-1} to O-H bending [32]. 1213 and 1022 cm^{-1} to asymmetric & symmetric C-N of acrylamide bending [31]. Such bands present in {P(Am-AA)-MgSi} composite indicates a good interaction of MgSi with P(Am-AA). 1104, 793, 611 & 465 cm^{-1}, to Si-O [16, 33] or Si-O-Si, Si-OH deformation vibration [16, 26] or Si–C transverse optical mode, Si-O-Mg [16, 26], and Si-H, respectively [35]. A fourth later absorption bands confirmed that impregnation of Mg & Si in a structure of polymeric resin. Such spectra showed good interactions of MgSi with P(Am-AN) & P(Am-AA) composites.

3.2 Morphological Features

The surface micrographs of the samples are observed in Fig. 2. It can be observed that well-mixed MgSi particles in the polymeric samples. A minimal amount of porosity might be noticed, whereas grains lean towards being fused between the grain boundaries. The samples of {P(Am-AA)-MgSi} & {P(Am-AN)-MgSi} were constituted as accumulated grains with a high variation of grain dimensions. The polymer grains appear to be decorated with crystals-like particles embedded within the polymeric grains. These particles may be assigned to the MgSi existence. Besides, we can notice that some agglomerated grains of MgSi crystalline particles are shown on the surface of the polymer grains. Figure 2(b,c) expresses the smoothness and homogeneity of the polymers of P(Am-AA) & P(Am-AN).

3.3 Ultrasonic Mechanical Characterization

The prepared samples' mechanical behavior was studied by the UT technique, and the results are presented in Fig. 3. The longitudinal, shear, Young's, and bulk moduli show the highest values of 12.22, 3.61, 7.41, and 9.32 GPa for the {P(Am-AN)-MgSi} sample compared to the other samples. This effect might be attributed to the good interfacial connections at the grain level between MgSi and P(Am-AN). The effect of mixing P(Am-AA) with higher E and G moduli of 7.89 and 3.10 GPa to MgSi with lower E and G of 5.31, and 2.04 GPa are presented in the {P(Am-AA)-MgSi} sample and reveals a midway of 7.13, and 2.71 GPa for E and G. Unlike the mixture of MgSi to P(Am-AN) the E and G shows an improved behavior for the {P(Am-AN)-MgSi} sample. The same behavior is represented for the microhardness of the samples with the highest value of 0.505 GPa for {P(Am-AN)-MgSi} sample compared to 0.269 & 0.274 for MgSi & P(Am-AN) initial component. The {P(Am-AN)-MgSi} microhardness performance might be explained by the best dispersion of MgSi in the P(Am-AA) polymer and resulting in lower porosity. From the results shown in Table 2, the composite contains P(Am-AN) has higher mechanical behavior than the composite contains P(Am-AA), while the neat polymers are not the same case [13]. The neat polymer of P(Am-AA) has shown a higher module than the P(Am-AN) due to its higher density of P(Am-AA) compared to P(Am-AN). A higher elastic modulus should present for the denser materials.

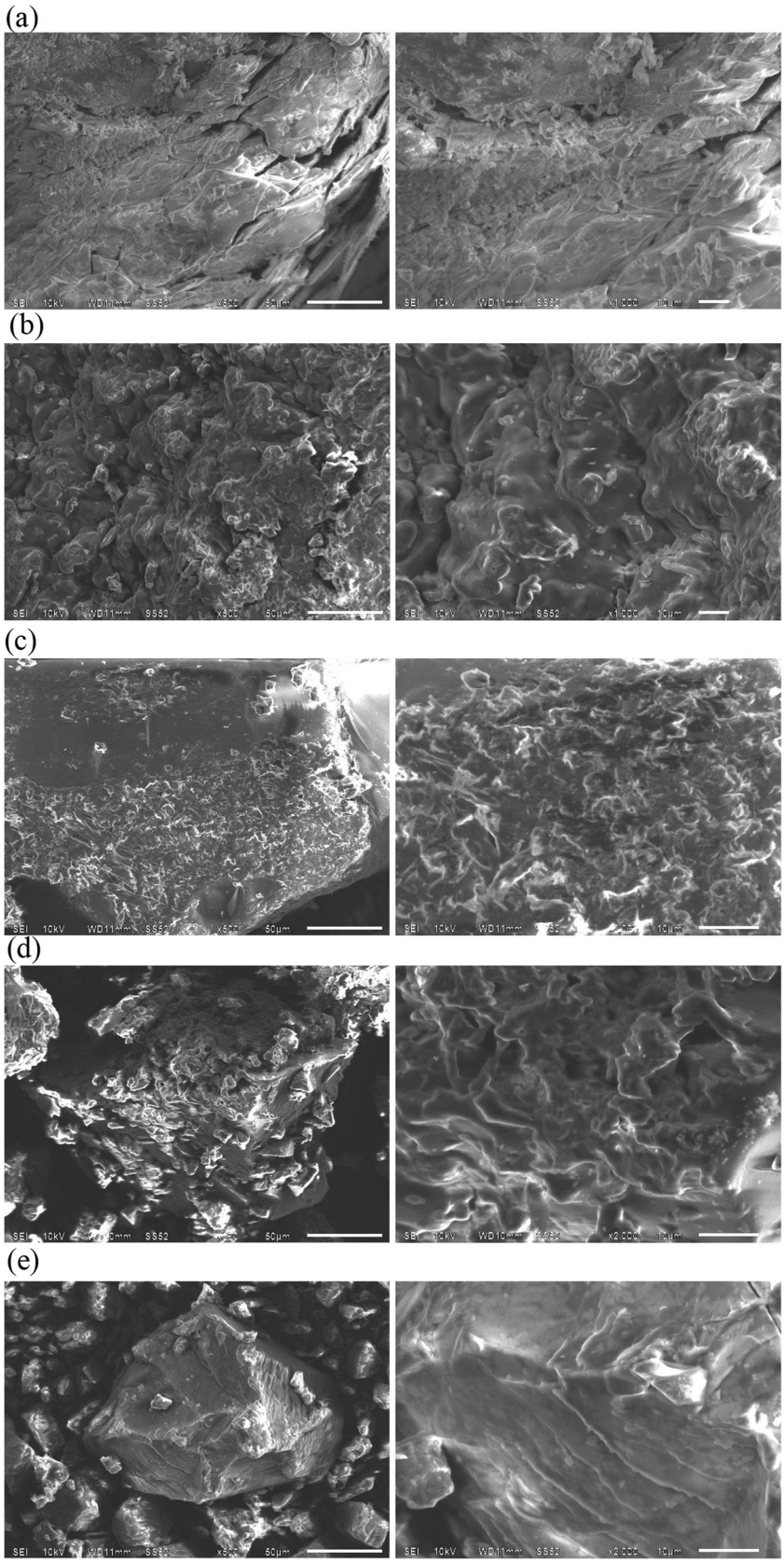

Fig. 2 SEM micrographs of (**a**) MgSi, (**b**) P(Am-AA), (**c**) P(Am-AN), (**d**) {P(Am-AA)-MgSi}, and (**e**) {P(Am-AN)-MgSi}

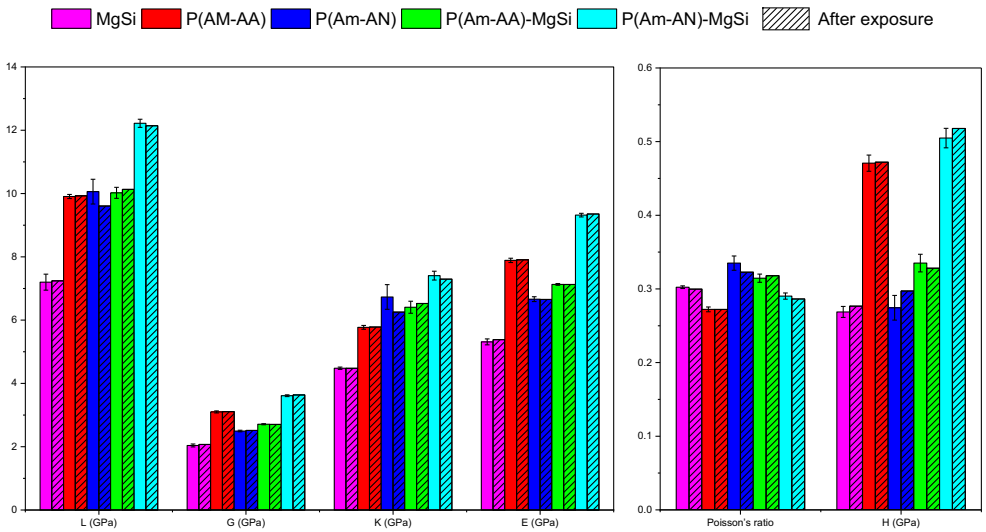

Fig. 3 The variation of the ultrasonic mechanical properties for all samples before (plain color columns) and after (patterned color columns) exposure with high power ultrasonic waves

Nevertheless, because of porosity or material defects, the composites of both polymers got reverse behavior. The porosity increases the internal stress in spotted areas inside the materials [18].

The compressed discs compatibility was investigated in terms of mechanical behavior before and after hitting with 40 W high power ultrasonic waves for 10 min each. We used silicon oil as a coupling media. The high-power waves might disintegrate the particles on the surface and near the surface. Also, it might cause a sample deformation. As shown in Fig. 3; Table 3, the elastic module, Poison's ratio, and microhardness remain within the standard deviation variation of the before exposure data. This indicates the discs are compatible and can resist the mechanical reaction caused by the high power coercivity, and can be utilized for radiation dosimetry.

3.4 Thermoluminescence Dosimetry

Figure 4 represents the characteristics of glow curves for the prepared samples at different irradiated doses from 0.5 Gy up to 2 Gy. Figure 4a shows a strong glow peak for MgSi arises at 205 °C without any changes in the peak location when different applied doses, which suggested this peak for detecting and monitoring the doses. TL response enhanced after added MgSi to (Am-AA) to form {P(Am-AA)-MgSi} compounds; this may have resulted from the creation of wide traps area, which is responsible for response increment as shown in Fig. 4d. The intense glow peak arises at 205 °C without any location movements with different doses, suggesting this peak for monitoring the doses [22]. TL response enhanced but little less than {P(Am-AA)-MgSi} after added MgSi to (Am-AN) to form {P(Am-AN)-MgSi} compounds, this may be attributed to the creation of wide traps area, which is responsible for the increased of response. A strong glow peak arises at 230 °C without any changes in the location with different doses, which suggested this peak for monitoring the doses. A strong glow peak arises at 225 °C without any changes in the location with different doses, which suggested this peak for monitoring the doses as in Fig. 4b for sample P(Am-AA).

The relations of the integral value of the TL-response for different testing materials are presented in Fig. 5. From the relations, we could find the individual polymer has lower doses response than the combined system, which enhances the integral value of the TL-response after combination with magnesium silicate. Consequently, Fig. 6 displays the relation of the peak height value of the TL-response for different testing

Table 2 The variation of ultrasonic mechanical properties of prepared samples

Samples	L (GPa)	G (GPa)	K (GPa)	E (GPa)	ν	H (GPa)
MgSi	7.20±0.253	2.04±0.047	4.48±0.037	5.31±0.094	0.30±0.002	0.27±0.007
P(Am-AA)	9.91±0.065	3.10±0.033	5.77±0.06	7.89±0.068	0.27±0.003	0.47±0.011
P(Am-AN)	10.06±0.391	2.49±0.025	6.73±0.389	6.66±0.077	0.34±0.010	0.27±0.017
{P(Am-AA)-MgSi}	10.02±0.173	2.71±0.018	6.41±0.19	7.13±0.028	0.32±0.006	0.34±0.012
{P(Am-AN)-MgSi}	12.22±0.128	3.61±0.028	7.41±0.139	9.32±0.057	0.29±0.004	0.51±0.013

Table 3 The mechanical properties of prepared samples after exposure with high power ultrasonic waves

Samples	L (GPa)	G (GPa)	K (GPa)	E (GPa)	ν	H (GPa)
MgSi	7.24	2.07	4.48	5.38	0.300	0.277
P(Am-AA)	9.93	3.11	5.78	7.91	0.272	0.472
P(Am-AN)	9.61	2.52	6.25	6.65	0.323	0.297
{P(Am-AA)-MgSi}	10.13	2.70	6.53	7.12	0.318	0.328
{P(Am-AN)-MgSi}	12.14	3.64	7.29	9.35	0.286	0.518

materials. The individual polymer has a lower dose-response than the combined system, which enhances the peak height value after combination with magnesium silicate. The lowest value is for MgSi then P(Am-AA) then P(Am-AN) then {P(Am-AA)-MgSi} & {P(Am-AN)-MgSi}[10]. The combination was affecting the response of both the height TL-response and integral value due to a combination of different traps to a

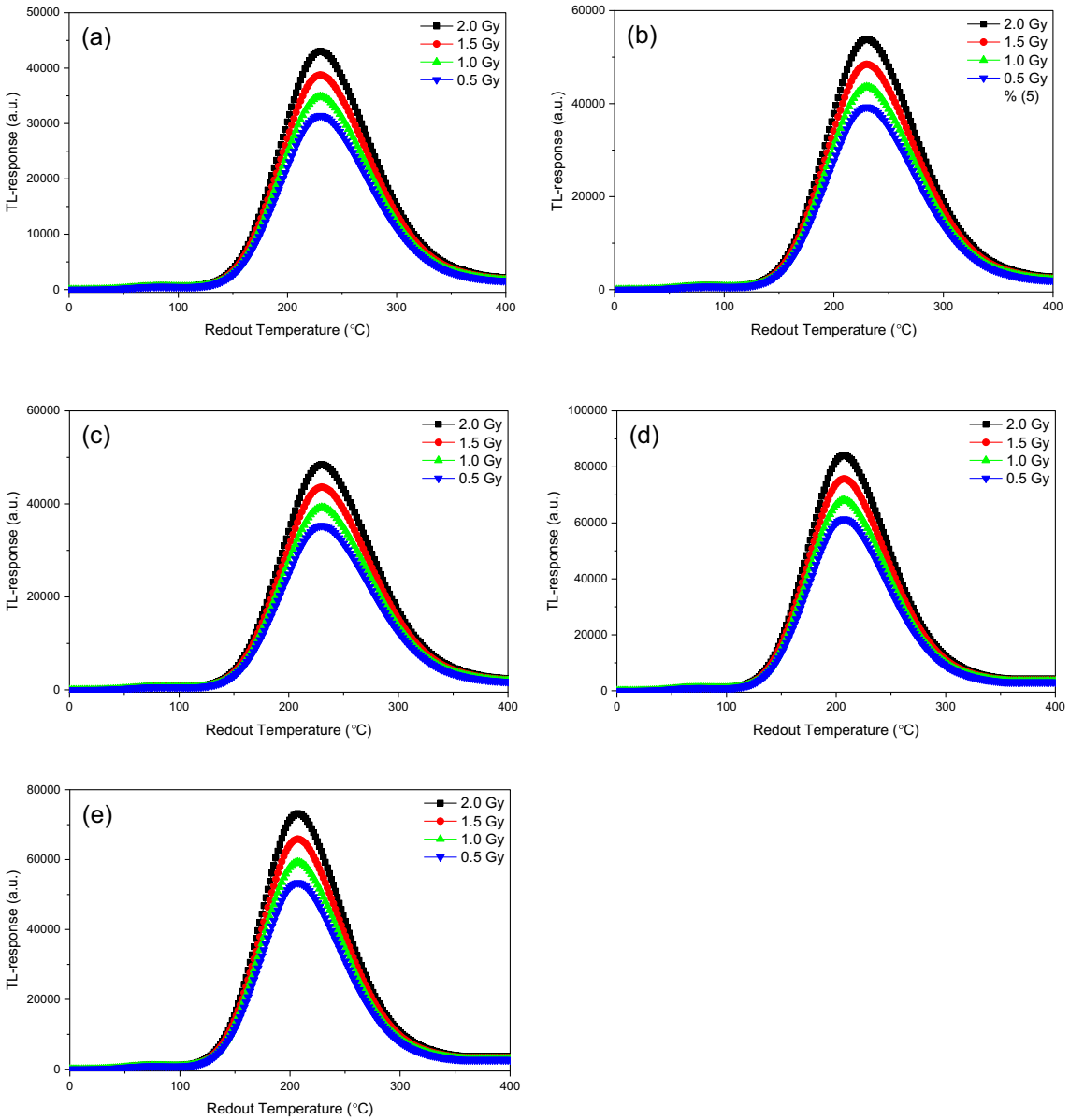

Fig. 4 The different glow curves of thermoluminescence of different doses for (**a**) MgSi, (**b**) P(Am-AA), (**c**) P(Am-AN), (**d**) {P(Am-AA)-MgSi}, and (**e**) {P(Am-AN)-MgSi}

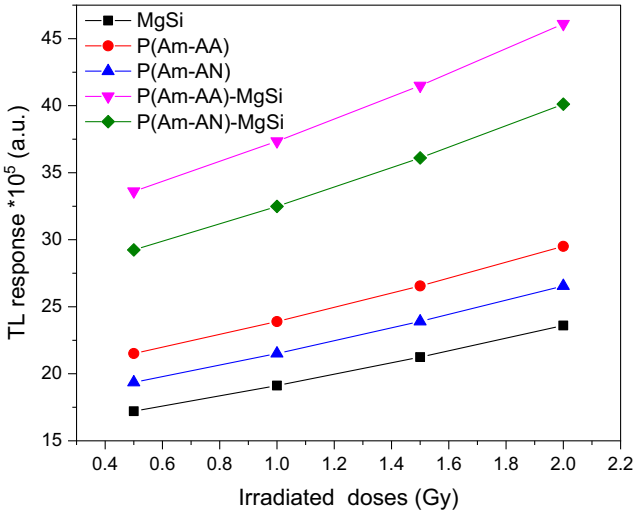

Fig. 5 TL dose-response as a function of integral value

confirmed wide area of traps suitable to probabilistic combination higher response.

Figure 7a represents the relationship between the fading time and the percentage TL intensity (%) for different polymeric materials [8]. The figure showed that the more fading polymeric material was P(AM-AN) and the less fading polymeric material one was P(Am-AA); when the glassy material added to the polymeric substance, the fading for {P(Am-AN)-MgSi} became less value, and this may be attributed to more deep traps created which resulted in the more stability of reading and this what is needed and required for the personnel dosimetry. Figure 7b represents the relationship of different energy in keV and the relative TL intensity (%) for different polymeric materials [10]. While energy changing, the response for all polymeric materials doesn't show a remarkable change in relative TL response even after added the glassy material to the polymeric substances. As known, the

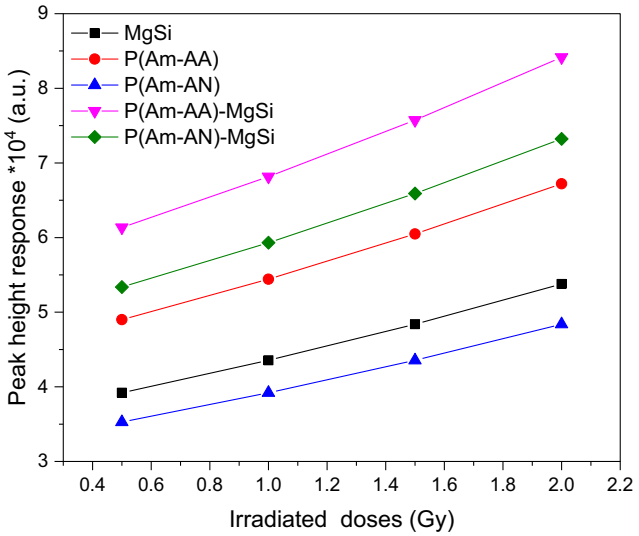

Fig. 6 TL dose-response as a function of peak height

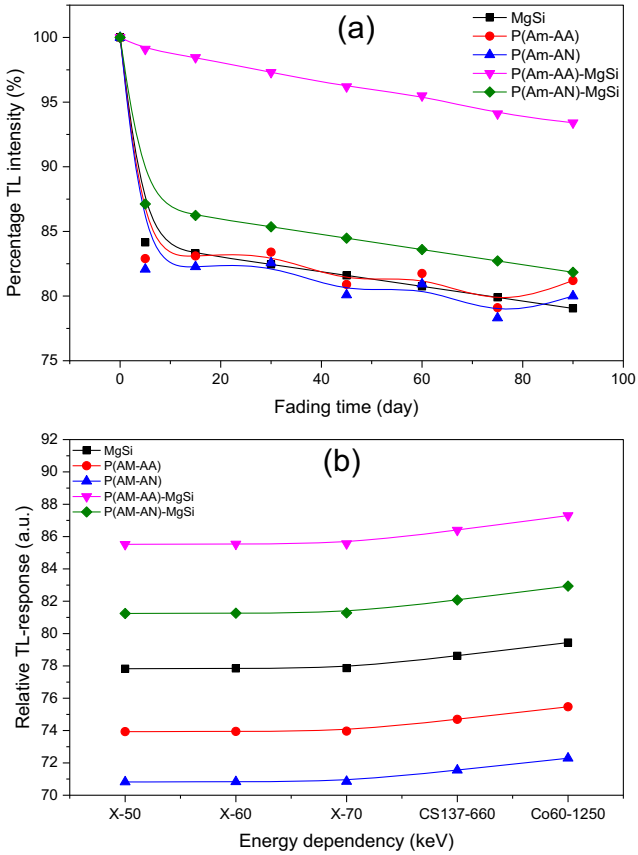

Fig. 7 (**a**) Variation of percentage TL intensity with fading time, and (**b**) The variation of relative TL response with energy dependency for the neat and composite samples

polymeric dosimetric materials should have energy-independent properties. i.e., no remarkable change in response even radiation energy changed so that all the polymeric materials under study were nominated to be dosimetric materials classes.

4 Conclusions

From previous results, a precipitation method was used to prepare MgSi. P(Am-AN), P(Am-AA), {P(Am-AN)-MgSi} & {P(Am-AA)-MgSi} composites have been prepared by 30 kGy gamma radiation dose subjected to co-monomers of Am, AN & AA for polymerization. The IR analysis data confirm the Mg & Si impregnation in the polymeric structure. From the test results, we can conclude that the samples show decent compatibility as they resist high-power ultrasonic mechanical wave deformations. Polymer composites are recommended to measure low gamma radiation dosed due to its good TL response of polymer samples after satisfied many of the requirements necessary for radiation dosimetry. Also, it could be concluded that when gamma dosimeter such as {P(Am-AA)-MgSi} & {P(Am-AN)-MgSi}is used for

measurements of the absorbed gamma dose, attention must be paid to the enhancement of TL response when combination occurred between the MgSi and the selected polymer. The polymers under study have adequate TL properties making them appropriate for gamma radiation dosimetric usage.

Author Contributions All authors contributed to the study conception and design.

Data Availability The authors mentioned all the relevant data associated with this research work in the manuscript and will be dedicated to sharing that they will be asked to do so in the future.

Declarations

Conflict of Interest The authors declare that they have no known conflict of interests.

Consent to Participate and Consent for Publication Not applicable.

References

1. Mirzayev MN, Demir E, Mammadov KF et al (2020) Amorphisation of boron carbide under gamma irradiation. Pramana - J Phys 94:110. https://doi.org/10.1007/s12043-020-01980-3
2. Mirzayev MN (2020) Oxidation kinetics of boron carbide ceramic under high gamma irradiation dose in the high temperature. Ceram Int 46:2816–2822. https://doi.org/10.1016/j.ceramint.2019.09.273
3. Mirzayev MN, Jabarov SH, Asgerov EB et al (2019) X-ray diffraction and thermodynamics kinetics of SiB6 under gamma irradiation dose. Silicon 11:2499–2504. https://doi.org/10.1007/s12633-018-0039-2
4. Diab HM, Abdelghany AM, Hafez HS (2020). Dosimetric behavior of modified borate bioglass containing copper for low photon dose measurements using luminescence characteristics. J Mater Sci Mater Electron 31(22):20452–20459
5. Diab HM (2005). Luminescence properties of Sm3+ in strontium tetraborate for assessment of electron beam dosimetry. Radiat Eff Defects Solids 160(3–4):137–143
6. Bruzzi M, Bucciolini M, Cirrone GAP et al (1999) Characterization of CVD diamond films as radiation detectors for dosimetric applications. In: 1999 IEEE Nuclear Science Symposium. Conference Record. 1999 Nuclear Science Symposium and Medical Imaging Conference (Cat. No. 99CH37019). IEEE, New York, pp 121–124
7. Bloemen-van Gurp E, Du Bois W, Visser P et al (2003) Clinical dosimetry with MOSFET dosimeters to determine the dose along the field junction in a split beam technique. Radiother Oncol 67: 351–357
8. Diab HM (2003) Standardization, calibration and development of some dosimeters using different techniques, Ph.D. Thesis, Cairo University
9. Andreo P, Cunningham JC, Hohlfeld K, Svensson H (1997) Absorbed dose determination in photon and electron beams. An International Code of Practice IAEA Technical Report Series No. 277. Int At Energy Agency, Vienna
10. Diab HM, Ibrahim A, El-Mallawany R (2013) Silicon solar cells as a gamma ray dosimeter. Measurement 46:3635–3639
11. Abd-Elghany AA, Diab HM, Sulieman A (2020) Determination of electron radiation dose uncertainty for strontium tetraborate doped with samarium. J Radiat Res Appl Sci 13:246–251
12. Elkhoshkhany N, Abbas R, Gaafar MS, El-Mallawany R (2015) Elastic properties of quaternaryTeO2–ZnO–Nb2O5–Gd2O3 glasses. Ceram Int 41:9862–9866. https://doi.org/10.1016/j.ceramint.2015.04.060
13. Gaafar MS, Marzouk SY, Mahmoud IS, et al (2020) Influence of samarium on some acoustical, physical and radiation shielding characteristics of Bi_2O_3–ZnO–PbO glasses. J Mater Sci Mater Electron 31:21502–21514. https://doi.org/10.1007/s10854-020-04663-2
14. El-Mallawany R, Diab HM (2012) Improving dosimetric properties of tellurite glasses. Phys B Condens Matter 407:3580–3585
15. El-Mallawany R, Diab HM (2013) Effect of pre-readout annealing treatments on TL mechanism in tellurite glasses at therapeutic radiation doses level. Measurement 46:1722–1725
16. Abou-Mesalam MM, Abass MR, Abdel-Wahab MA et al (2016) Complex doping of d-block elements cobalt, nickel and cadmium in magneso-silicate composite and its use in the treatment of aqueous waste. Desalin Water Treat 57:25757–25764
17. Abou-Mesalam MM, Abass MR, Ibrahim AB et al (2019) Tunable optical and dielectric properties of polymeric composite materials based on magneso-silicate. Bull Mater Sci 42:31
18. Mansour SFF, Eid AMM, El-Latif LAA et al (2017) Structure, ferroelectric and mechanical performance of polycrystalline gadolinium-doped lead lanthanum zirconate titanate ceramics. In: 2017 Joint IEEE International Symposium on Applications of Ferroelectrics, International Workshop on Acoustic Transduction Materials and Devices and Piezoresponse Force Microscopy Workshop, ISAF-IWATMD-PFM 2017 - Conference. IEEE, New York, pp 63–67
19. Gaafar MS, Marzouk SY, Mahmoud IS et al (2020) Role of neodymium on some acoustic and physical properties of Bi2O3 - B2O3- SrO glasses. J Mater Res Technol. https://doi.org/10.1016/j.jmrt.2020.04.086
20. IAEA (1994) (International Atomic Energy Agency), Calibration of dosimeters used in radiotherapy: an international code of practice, Technical Report Series No. 374, IAEA, Vienna
21. IAEA (1997) (International Atomic Energy Agency), The use of plane parallel ionization chambers in high energy electron and photon beams - an international code of practice for dosimetry, Technical Report Series No. 381, IAEA, Vienna
22. Abass MR, Diab HM, Abou-Mesalam MM (2021) New improved thermoluminescence magnesium silicate material for clinical dosimetry. Silicon 1–9. https://doi.org/10.1007/s12633-021-01049-9
23. Ali IM, Kotp YH, El-Naggar IM (2010) Thermal stability, structural modifications and ion exchange properties of magnesium silicate. Desalination 259:228–234
24. Al-Degs YS, El-Barghouthi MI, Issa AA et al (2006) Sorption of Zn (II), Pb (II), and Co (II) using natural sorbents: equilibrium and kinetic studies. Water Res 40:2645–2658
25. Madejová J (2003) FTIR techniques in clay mineral studies. Vib Spectrosc 31:1–10
26. Nabi SA, Shahadat M, Bushra R et al (2011) Synthesis and characterization of nano-composite ion-exchanger; its adsorption behavior. Colloids Surfaces B Biointerfaces 87:122–128
27. Al-Yassir N, Le Van Mao R (2007) Catalysts for the thermocatalytic cracking (TCC) process: Interactions between the yttria in yttria-doped alumina aerogel and the mono-oxide MoO3, CeO2, and bi-oxide MoO3–CeO2 species. Appl Catal A Gen 332:273–288
28. Lee S, Kim JJ, Ku B-C et al (2012) Structural evolution of polyacrylonitrile fibers in stabilization and carbonization. 275–282. https://doi.org/10.4236/aces.2012.22032

29. Saufi SM, Ismail AF (2002) Development and characterization of polyacrylonitrile (PAN) based carbon hollow fiber membrane. Songklanakarin J Sci Technol 24:843–854
30. Wang Q, Dong Z, Du Y, Kennedy JF (2007) Controlled release of ciprofloxacin hydrochloride from chitosan/polyethylene glycol blend films. Carbohydr Polym 69:336–343
31. Hassan MF, Yusof SZM (2014) Poly (acrylamide-co-acrylic acid)-zinc acetate polymer electrolytes: Studies based on structural and morphology and electrical spectroscopy. Microsc Res 2:30
32. Dawood AS, Li Y (2014) Wastewater flocculation using a new hybrid copolymer: Modeling and optimization by response surface methodology. Polish J Environ Stud 23:43–50
33. Borai EH, Hamed MG, El-Kamash AM et al (2015) Synthesis, characterization and application of a modified acrylamide–styrene sulfonate resin and a composite for sorption of some rare earth elements. New J Chem 39:7409–7420
34. Li D, Wang M, Yang C et al (2012) Solid state characterizations and analysis of stability in azelnidipine polymorphs. Chem Pharm Bull 60:995–1002
35. Mirzayev MN, Abdurakhimov BA, Demir E et al (2021) Investigation of the formation of defects under fast neutrons and gamma irradiation in 3 C–SiC nano powder. Phys B Condens Matter 611:412842. https://doi.org/10.1016/j.physb.2021.412842
36. Semagne B, Diaz I, Kebede T, Taddesse AM (2016) Synthesis, characterization and analytical application of polyaniline tin (IV) molybdophosphate composite with nanocrystalline domains. REACT 98:17–23. https://doi.org/10.1016/j.reactfunctpolym.2015.11.004
37. Silverstein RM, Webster FX, Kiemle DJ, Bryce DL (2014) Spectrometric identification of organic compounds. Wiley, Hoboken
38. Abdel-Galil EA, Rizk HE, Mostafa AZ (2016) Production and characterization of activated carbon from Leucaena plant wastes for removal of some toxic metal ions from waste solutions. Desalin Water Treat 57:17880–17891
39. Abou-Mesalam MM, El-Naggar IM (2008) Selectivity modification by ion memory of magneso-silicate and magnesium alumino-silicate as inorganic sorbents. J Hazard Mater 154:168–174

Publisher's Note Springer Nature remains neutral with regard to jurisdictional claims in published maps and institutional affiliations.